Transcriptional control of lung alveolar type 1 cell development and maintenance by NK homeobox 2-1

Danielle R. Little[a,b], Kamryn N. Gerner-Mauro[a], Per Flodby[c], Edward D. Crandall[c], Zea Borok[c], Haruhiko Akiyama[d], Shioko Kimura[e], Edwin J. Ostrin[a,f], and Jichao Chen[a,1]

[a]Department of Pulmonary Medicine, The University of Texas MD Anderson Cancer Center, Houston, TX 77030; [b]University of Texas Health Graduate School of Biomedical Sciences, The University of Texas MD Anderson Cancer Center, Houston, TX 77030; [c]Division of Pulmonary, Critical Care and Sleep Medicine, Department of Medicine and Hastings Center for Pulmonary Research, Keck School of Medicine, University of Southern California, Los Angeles, CA 90033; [d]Department of Orthopedics, Kyoto University, Sakyo, 606-8507 Kyoto, Japan; [e]Laboratory of Metabolism, Center for Cancer Research, National Cancer Institute, National Institutes of Health, Bethesda, MD 20892; and [f]Department of General Internal Medicine, The University of Texas MD Anderson Cancer Center, Houston, TX 77030

Edited by Clifford J. Tabin, Harvard Medical School, Boston, MA, and approved August 30, 2019 (received for review April 18, 2019)

The extraordinarily thin alveolar type 1 (AT1) cell constitutes nearly the entire gas exchange surface and allows passive diffusion of oxygen into the blood stream. Despite such an essential role, the transcriptional network controlling AT1 cells remains unclear. Using cell-specific knockout mouse models, genomic profiling, and 3D imaging, we found that NK homeobox 2-1 (*Nkx2-1*) is expressed in AT1 cells and is required for the development and maintenance of AT1 cells. Without *Nkx2-1*, developing AT1 cells lose 3 defining features—molecular markers, expansive morphology, and cellular quiescence—leading to alveolar simplification and lethality. NKX2-1 is also cell-autonomously required for the same 3 defining features in mature AT1 cells. Intriguingly, *Nkx2-1* mutant AT1 cells activate gastrointestinal (GI) genes and form dense microvilli-like structures apically. Single-cell RNA-seq supports a linear transformation of *Nkx2-1* mutant AT1 cells toward a GI fate. Whole lung ChIP-seq shows NKX2-1 binding to 68% of genes that are down-regulated upon *Nkx2-1* deletion, including 93% of known AT1 genes, but near-background binding to up-regulated genes. Our results place NKX2-1 at the top of the AT1 cell transcriptional hierarchy and demonstrate remarkable plasticity of an otherwise terminally differentiated cell type.

lung development | alveolar type 1 cell | NK homeobox 2-1 | transcriptional control | alveologenesis

Cells often undergo morphological and molecular specialization to fulfill their physiological function, such as neurons, cardiomyocytes, and pancreatic beta cells. The cell type chiefly responsible for the physiological function of the lung—gas exchange—is the alveolar type 1 (AT1) cell. AT1 cells cover 95% of the gas exchange surface and are 0.1 μm thick to allow passive diffusion of oxygen into the blood stream. They have expansive morphology, covering multiple alveoli, and fold extensively, forming close contact with the vasculature (1–5). Unlike the AT1 cell, the alveolar type 2 (AT2) cell, the other major cell type of the alveolar epithelium, is cuboidal and secretes surfactants to reduce surface tension (1, 2).

The unique morphology of AT1 cells develops in 2 steps (5). First, it undergoes flattening from a columnar progenitor. Then, it expands >10-fold in size and at the same time folds to interdigitate with the capillaries. Growing evidence indicates that both tissue environment, such as mechanical forces and extracellular matrix, and intracellular factors could impact AT1 cell development. For example, reducing mechanical tension from fetal breathing by depleting the amniotic fluid or lowering the stiffness of cell culture surface favors AT2 over AT1 cell differentiation (6). Loss of an extracellular matrix protein, COL4A1, also leads to an increased ratio of AT2 to AT1 cells (7). Inside the epithelial cells, beta-catenin–mediated canonical WNT signaling as well as fibroblast growth factor signaling inhibit AT1 cell differentiation (6, 8–10) and HDAC3-dependent TGF-beta signaling is required for proper epithelium expansion and AT1 cell spacing (8, 11). More recently, genetic analyses of *Mst1/2*, *Lats1/2*, and *Yap/Taz* indicate that Hippo signaling promotes progenitor differentiation toward the AT1 cell fate (12–14). This growing list of AT1 cell regulators highlights both the underlying complexity and the necessity to distinguish direct effects on AT1 cells versus those on progenitors, AT2 cells, or tissue morphology, especially in light of the classical observation of rapid AT1 cell-like differentiation of cultured AT2 cells (15). A better understanding of AT1 cell development also requires identification of sequence-specific transcription factors that activate AT1 cell-specific genes and cellular machinery that determines its unique morphology.

In a previous model to disrupt AT1 cell development, we ectopically expressed the airway transcription factor SRY-box 2 (SOX2) in developing AT1 cells. These mutant cells became airway-like in association with drastic molecular and morphological changes, prompting the question of whether they retained the lung fate, which we addressed by immunostaining for the lung lineage transcription factor NKX2-1 (5). To our surprise, AT1 cells in the control lung had nuclear NKX2-1, different from prior reports that NKX2-1 is a lineage factor during lung specification and branching morphogenesis, but is lost in AT1 cells upon alveolar differentiation (16, 17). Intriguingly, NKX2-1 staining in SOX2-expressing mutant AT1 cells was diffuse instead of nuclear,

Significance

Gas exchange in the lung relies on passive diffusion of oxygen and carbon dioxide across an extraordinarily thin epithelium that is nearly entirely made of the poorly understood alveolar type 1 (AT1) cell. Our study shows that all AT1 cells express and require NK homeobox 2-1 (*Nkx2-1*) for their development and maintenance. *Nkx2-1* mutant AT1 cells lose their characteristic molecular and cellular features and transform toward a gastrointestinal fate, highlighting remarkable plasticity of an otherwise terminally differentiated cell type. This work establishes NKX2-1 as the first overarching factor in the AT1 cell transcriptional hierarchy and paves the way for unraveling not only the unique biology of AT1 cells but also cell type-specific roles of a lineage transcription factor.

Author contributions: D.R.L. and J.C. designed research; D.R.L. and K.N.G.-M. performed research; P.F., E.D.C., Z.B., H.A., and S.K. contributed new reagents/analytic tools; D.R.L., K.N.G.-M., and E.J.O. analyzed data; and D.R.L. and J.C. wrote the paper.

The authors declare no conflict of interest.

This article is a PNAS Direct Submission.

Data deposition: The data reported in this paper have been deposited in the Gene Expression Omnibus (GEO) database, www.ncbi.nlm.nih.gov/geo (accession no. GSE129628).

[1]To whom correspondence may be addressed. Email: jchen16@mdanderson.org.

This article contains supporting information online at www.pnas.org/lookup/suppl/doi:10.1073/pnas.1906663116/-/DCSupplemental.

First published September 23, 2019.

as expected for a transcription factor, raising the possibility that NKX2-1 regulates AT1 cell development.

In this study, we use precise genetic deletion models and genomic analyses to show that NKX2-1 is necessary for the initiation, development, and maintenance of AT1 cells. *Nkx2-1* mutant AT1 cells lose 3 defining features—AT1 cell-specific markers, morphology, and quiescence—and aberrantly express gastrointestinal (GI) genes. This study establishes NKX2-1 as a key transcription factor controlling AT1 cells.

Results

NKX2-1 in AT1 Cells Is Required for Alveologenesis. To confirm and extend knowledge of NKX2-1 expression in AT1 cells, we genetically marked all lung epithelial cell nuclei, including those of AT1 and AT2 cells, with a Shh^{Cre} driver (18) and a nuclear Cre reporter, $Rosa^{Sun1GFP}$ (19). To visualize the expansive AT1 cells in their entirety, we used whole mount immunostaining and confocal stack imaging of strips cut from lobe edges (ref. 5 and Fig. 1*A*). In such preparations, AT1 and AT2 cells appeared as a "fried egg" and an "egg in the shell," respectively, as outlined by an epithelial junction protein E-cadherin (ECAD) (Fig. 1*A*). We found that throughout postnatal development as well as in the mature lung, NKX2-1 was present in every single green fluorescent protein (GFP)-labeled cell, corresponding to both AT1 and AT2 cells, which were further distinguished by an AT2 marker, lysosome-associated membrane protein 3 (LAMP3) (Fig. 1*B*). Thus, instead of being lost upon AT1 cell differentiation as suggested previously (16, 17), NKX2-1 is expressed in both developing and mature AT1 cells.

Given the importance of NKX2-1 in early development (20–22) and its aberrant localization in the SOX2 ectopic expression model, as described in the introduction (5), we hypothesized that NKX2-1 had a role in AT1 cell development. To test this, we generated an AT1 cell-specific knockout of *Nkx2-1* using an $Aqp5^{Cre}$ driver (23, 24). A portion of these mice had widespread expression of a GFP reporter across organs, possibly due to early recombination during embryogenesis or within the parental germline, and were thus excluded from analysis. In the remaining mice, $Aqp5^{Cre}$ targeted AT1 cells with an efficiency of 96% and specificity of 98% within the alveolar epithelium at postnatal day

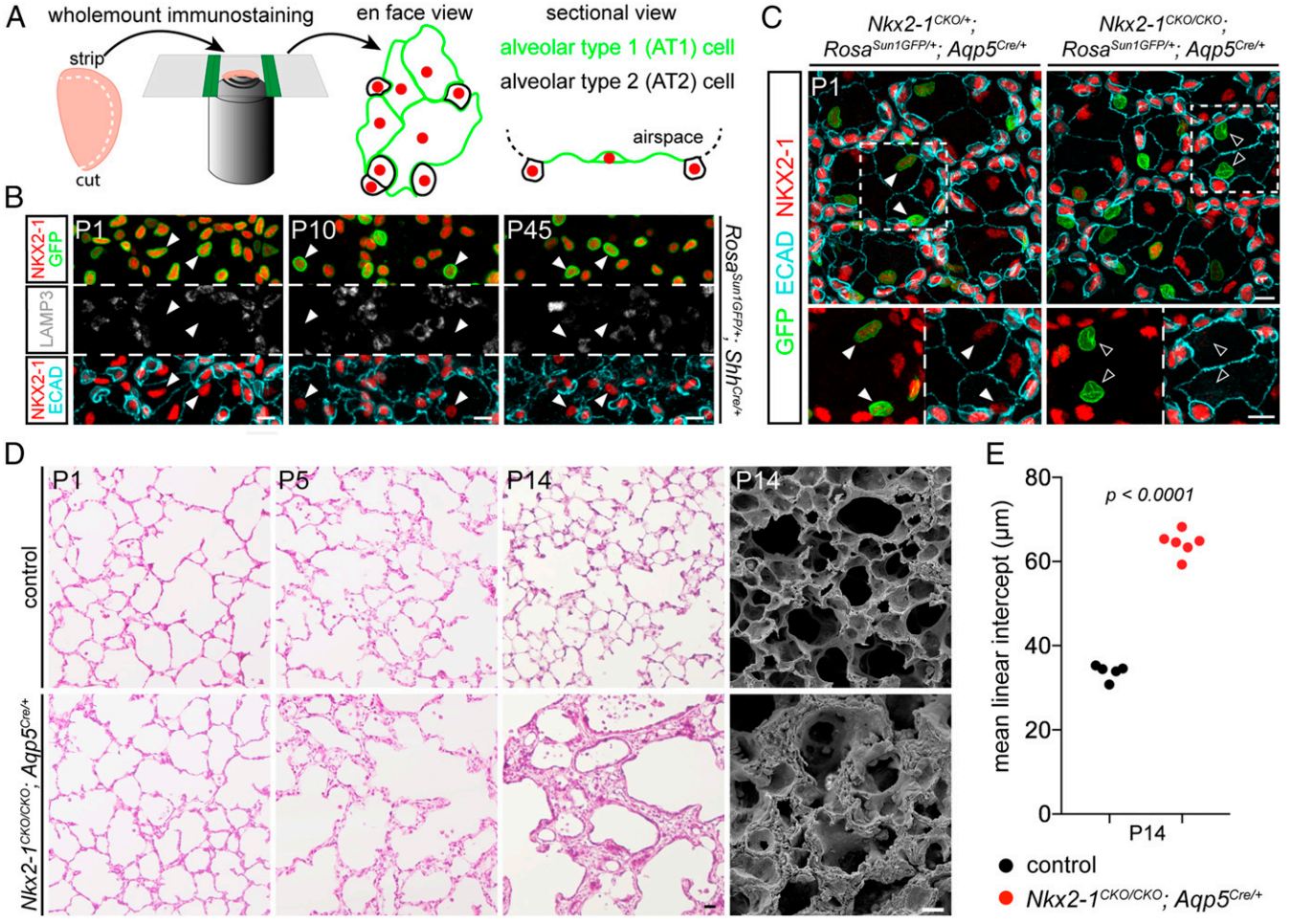

Fig. 1. NKX2-1 is required in AT1 cells for alveologenesis. (*A*) Schematics of sample preparation to obtain an en face view of complete AT1 cells (traced from an immunostained P3 lung), whose conventional sectional view captures part of a cell as a line bordering the airspace. (*B*) Confocal en face view of immunostained $Rosa^{Sun1GFP/+}$; $Shh^{Cre/+}$ lung strips showing that NKX2-1 is expressed by all epithelial cells, whose nuclei are genetically marked with GFP, including all AT1 cells as identified by the expanded cell size outlined by ECAD and absence of LAMP3 (arrowheads). At least 2 mice were examined at each time point with consistent results. (*C*) Confocal en face view of immunostained littermate lung strips showing specific loss of NKX2-1 in GFP-marked, expanded AT1 cells in the mutant (open versus filled arrowheads). At least 3 lungs per genotype were examined with consistent results. (*D*) *Left* 3 columns: H&E stained sections from littermate lungs. At least 3 lungs per genotype were examined with consistent results. *Rightmost* column: scanning electron microscopy images of littermate lungs. (*E*) *Nkx2-1* mutant lungs have an increased mean linear intercept (unpaired *t* test). Each dot represents 1 lung averaged over 5 images. (Scale bars: 10 μm in *B* and *C*; 20 μm in *D*.)

(P) 5 based on the $Rosa^{Sun1GFP}$ reporter (n = 3 mice; >1,100 cells/mouse). Recombination was also seen in occasional non–NKX2-1 expressing, flat cells on the lobe surface, which were presumably mesothelial cells. NKX2-1 was lost in 93% of GFP-expressing AT1 cells at P5 (n = 3 mice, >700 GFP cells/mouse) with deletion observed as early as P1 (Fig. 1*C*). The resulting *Nkx2-1* mutant mice were visibly smaller starting from P7 and died between P14 and P23. H&E staining showed that the mutant lung had enlarged airspaces, thickened septa, and fewer alveoli (Fig. 1*D*). These morphological changes were confirmed with scanning electron microscopy (SEM) (Fig. 1*D* and *SI Appendix*, Fig. S1*A*). Mean linear intercept, which measures the average alveolar space size without distinguishing alveolar ducts, alveolar sacs, and alveoli, was significantly increased in the mutant (Fig. 1*E*). Thus, loss of NKX2-1 in developing AT1 cells disrupts alveologenesis and leads to lethality.

NKX2-1 Is Necessary for 3 Defining Features of Developing AT1 Cells. Next, we examined the molecular and cellular changes underlying the described mutant phenotypes. Immunostaining of $Rosa^{L10GFP}$ (25) lineage-labeled lungs showed that *Nkx2-1* mutant AT1 cells down-regulated 4 AT1 cell markers: homeodomain-only protein (HOPX), advanced glycosylation end product-specific receptor (AGER or RAGE), podoplanin (PDPN), and aquaporin 5 (AQP5) (Fig. 2*A* and *SI Appendix*, Fig. S1*B*). Unlike membrane-localized AT1 markers, HOPX was present in the nucleus and allowed reliable quantification,

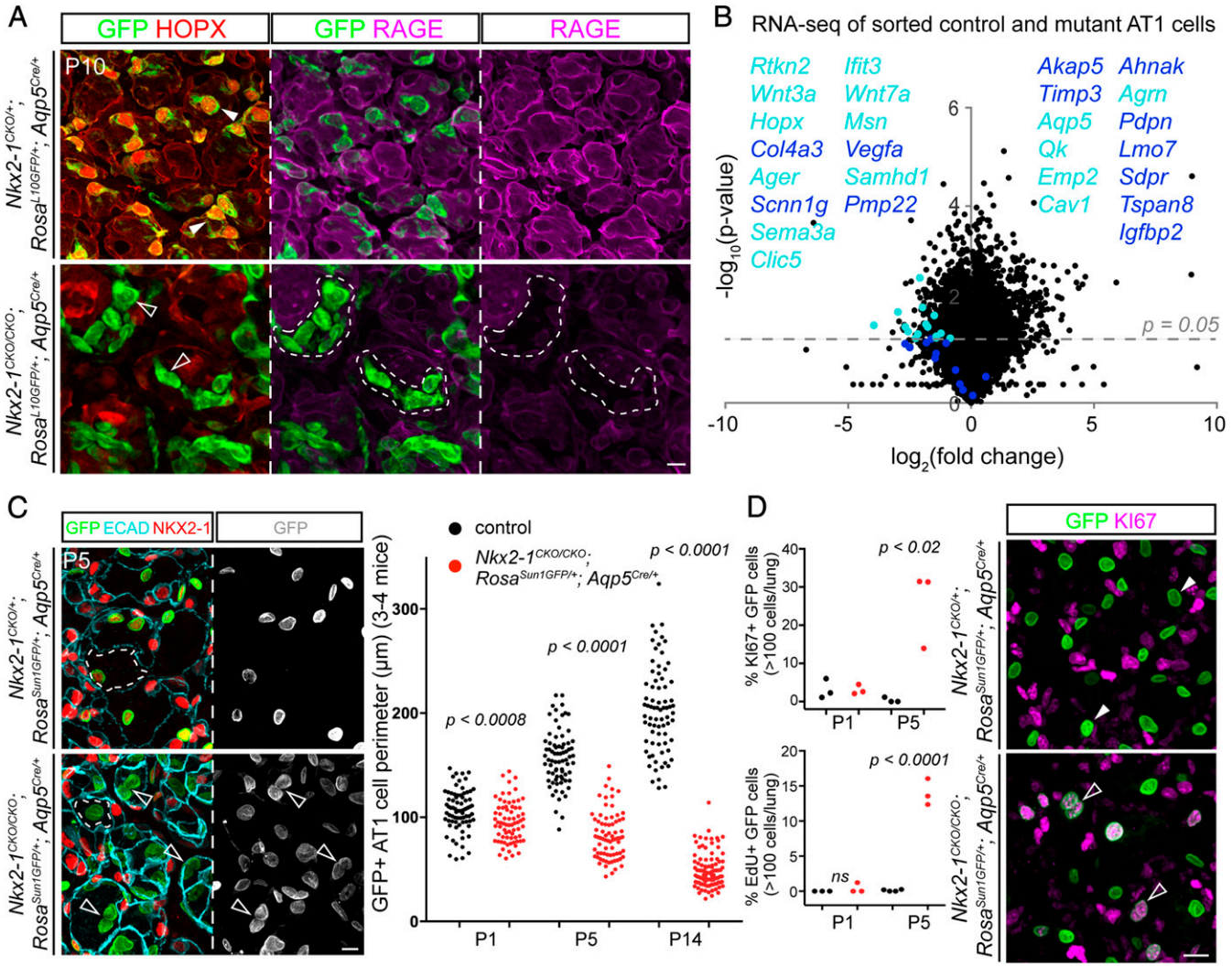

Fig. 2. NKX2-1 is necessary for AT1 cell gene expression, morphology, and quiescence. (*A*) Confocal en face view of immunostained littermate lung strips showing reduced AT1 cell markers in GFP-marked AT1 cells in the mutant, including HOPX (open versus filled arrowheads) and RAGE (dashed outline). Mutant cell patches are small because mutant cells shrink (below) and are outcompeted in size by neighboring control cells. The L10GFP reporter is cytosolic and only appears perinuclear because there is a larger amount of cytosol around the nucleus of flattened AT1 cells. At least 3 littermate pairs were examined with consistent results. (*B*) Volcano plot of RNA-seq comparison of sorted GFP-marked AT1 cells from 3 pairs of P5 $Nkx2\text{-}1^{CKO/CKO}$; $Rosa^{L10GFP/+}$; $Aqp5^{Cre/+}$ mutant and littermate control lungs (paired *t* test). AT1 cell genes (cyan) are highlighted in the plot and listed in the order of fold change (all 4 columns; top to bottom and then left to right); darker cyan indicates genes below the $P = 0.05$ line of statistical significance. (*C*) Confocal en face view of immunostained littermate lung strips showing a decrease in the cell perimeter of GFP-marked NKX2-1 mutant AT1 cells, as outlined by ECAD (dashes) and as quantified at indicated time points with each dot representing a cell from at least 3 lungs per genotype with 5 images per lung (unpaired *t* test). Open arrowheads indicate binuclear (outlined by GFP) mutant AT1 cells. (*D*) Confocal en face view of immunostained littermate lung strips showing KI67 expression in GFP-marked AT1 cells in the mutant (open versus filled arrowheads), as quantified at indicated time points with each dot representing 1 lung averaged over 3 images (unpaired *t* test; *Top* plot). Aberrant proliferation was confirmed by EdU staining with each dot representing 1 lung averaged over at least 4 images (unpaired *t* test; ns, not significant; *Bottom* plot). (Scale bars: 10 μm in *A*, *C*, and *D*.)

which showed expression in 28% of GFP cells in the mutant lung versus 95% in the control lung at P10 ($n = 3$ mice for each genotype; >700 GFP cells/mouse). To extend this analysis to all AT1 cell-specific genes that we compiled from the literature (5, 23, 26, 27), we performed RNA-seq of purified genetically labeled AT1 cells from P5 control and *Nkx2-1* mutant lungs. We found down-regulation of 25 out of 27 AT1 genes, such as *Sema3a*, *Clic5*, *Samhd1*, *Rtkn2*, *Cav1*, *Hopx*, *Ager*, and *Aqp5* (Fig. 2*B* and Dataset S1). Ten out of the 25 down-regulated AT1 genes did not reach statistical significance, possibly due to mosaic deletion of *Nkx2-1* and/or perdurance because one such gene, *Pdpn*, was lower on the protein level at a later time point (*SI Appendix*, Fig. S1*B*).

A second defining feature of AT1 cells is their thin and expansive cell morphology, which allows passive gas diffusion (3). Using the aforementioned whole mount immunostaining and imaging method to visualize complete AT1 cells, we found that, while control AT1 cells grew over time as reported (5), *Nkx2-1* mutant AT1 cells were smaller as early as P3 and continued to regress until becoming cuboidal at P14, as quantified by measuring the cell perimeter (Fig. 2*C* and *SI Appendix*, Fig. S1*C*). Interestingly, mutant AT1 cells accumulated a higher level of ECAD at the cell junctions, possibly as a result of transcriptional up-regulation and/or protein redistribution due to cell shrinkage (*SI Appendix*, Fig. S1*C*).

AT1 cells are generally considered quiescent and nonproliferative at baseline, especially considering their specialized morphology (5, 26, 28). Using the $Rosa^{Sun1GFP}$ nuclear reporter, we noticed that *Nkx2-1* mutant AT1 cells frequently exhibited a binuclear mitotic profile (Fig. 2 *C* and *D*). To determine if they reentered the cell cycle, we examined KI67, a nonquiescent cell marker, and EdU incorporation, an S phase readout, at multiple time points. Indeed, we found 30 and 15% of mutant AT1 cells were positive for KI67 and EdU, respectively, as compared to negligible percentages for control AT1 cells (Fig. 2*D* and *SI Appendix*, Fig. S1 *D* and *E*). Notably, proliferating mutant cells were seen as early as P3, when cell shrinkage just started and before loss of AT1 markers, suggesting a direct role of NKX2-1 in suppressing AT1 cell proliferation. Intriguingly, some mutant AT1 nuclei were also larger, as outlined by the nuclear GFP reporter (*SI Appendix*, Fig. S1*F*). This was perhaps due to a delay in mitosis after DNA replication, a possibility consistent with the aforementioned binuclear mitotic profile. These proliferating, small mutant AT1 cells formed clusters (*SI Appendix*, Fig. S1*C*); at P14, occasional mutant cells underwent apoptosis based on TUNEL staining (*SI Appendix*, Fig. S1*G*). No compensatory AT2 cell proliferation was observed at an advanced stage of the mutant phenotype (*SI Appendix*, Fig. S1*H*). Collectively, these data suggest that NKX2-1 is required for 3 defining features of AT1 cells: cell markers, morphology, and quiescence. Mutant AT1 cell shrinkage and proliferation led to a thick, compact epithelium, likely incompatible with alveologenesis and gas exchange.

NKX2-1 Regulates AT1 Cell Development in a Cell-Autonomous Manner. To independently validate the phenotypes and to exclude secondary effects from gross structural changes in the $Aqp5^{Cre}$ driven *Nkx2-1* deletion model, we used another AT1 cell driver, $Hopx^{CreER}$ (28), which had an efficiency of 11% and specificity of 99% within the alveolar epithelium based on the $Rosa^{mTmG}$ reporter (29) in neonatal lungs ($n = 3$ mice; >75 cells/mouse). We optimized the dose of tamoxifen so that *Nkx2-1* was lost in 38% of GFP-expressing AT1 cells 7 d after tamoxifen injection ($n = 3$ mice; >100 GFP cells/mouse), resulting in isolated mutant cells and grossly normal lung morphology (Fig. 3 *A* and *B*). Consistent with the $Aqp5^{Cre}$ deletion model, individual mutant AT1 cells lost AT1 cell markers: HOPX, whose expression was detected in 38% of GFP cells in the mutant lung versus 90% in the control lung ($n = 2$ mice for each genotype; >50 GFP cells/mouse), AGER, PDPN, and AQP5, indicating that NKX2-1 is cell-autonomously required for AT1 cell gene expression (Fig. 3*C* and *SI Appendix*, Fig. S2*A*). The discrepancy between the percentages of GFP cells losing NKX2-1 versus HOPX in the mutant was likely due to variations in recombination in this limited deletion model. Similarly, mutant AT1 cells underwent cell perimeter regression and accumulated ECAD even when surrounded by control AT1 cells (Fig. 3*D*). Mutant AT1 cells also proliferated as early as 3 d after Cre activation, as indicated by KI67 staining (Fig. 3*E*). We note that although $Hopx^{CreER}$ targets occasional AT2 cells, such mistargeting cannot account for the high frequency of mutant cells exhibiting the phenotypes. Thus, all 3 defining features of developing AT1 cells—cell markers, morphology, and quiescence—depend on the cell-autonomous function of NKX2-1.

NKX2-1 Is Necessary for AT1 Cell Flattening. By design, both AT1 drivers, $Aqp5^{Cre}$ and $Hopx^{CreER}$, induced recombination after commitment to the AT1 cell fate and thus spared the initiation stage of its differentiation (Fig. 1*C*). To test if NKX2-1 is required for the first step of AT1 cell differentiation, cell flattening, we used $Sox9^{CreER}$ (30) to target the embryonic epithelial progenitors at embryonic day (E) 15.5 before their differentiation into AT1 or AT2 cells. NKX2-1 was lost in 22% of epithelial cells in the mutant lung at E18.5 ($n = 2$ mice; >1,500 cells/mouse). While $Rosa^{L10GFP}$-labeled, recombined cells in the control lung consisted of both flattened AT1 cells and cuboidal/columnar AT2/progenitor cells, none of the *Nkx2-1* mutant cells flattened (*SI Appendix*, Fig. S3 *A* and *B*). *Nkx2-1* mutant lungs also had decreased expression of an AT1 cell gene PDPN, as well as an AT2 cell gene LAMP3, supporting a role of NKX2-1 in both AT1 and AT2 gene expression (*SI Appendix*, Fig. S3 *C* and *D*). While proliferation was normally low in late gestation lungs, *Nkx2-1* mutant lungs had increased expression of KI67 (*SI Appendix*, Fig. S3*E*). These data suggest that NKX2-1 is required to initiate AT1 cell flattening, gene expression, and quiescence.

NKX2-1 Is Necessary to Maintain AT1 Cell Fate in the Mature Lung. To test if NKX2-1 is still required in mature, fully specialized AT1 cells, we deleted *Nkx2-1* in 5-wk-old mice using $Hopx^{CreER}$, which targeted AT1 cells with an efficiency of 23% with a high dose of tamoxifen (6 mg) but had 100% specificity within the alveolar epithelium based on the $Rosa^{mTmG}$ reporter ($n = 3$ mice; >120 cells/mouse) (Fig. 4 *A* and *B*). In this deletion model, NKX2-1 was lost in 65% of GFP-expressing AT1 cells ($n = 3$; >100 GFP cells/mouse) (Fig. 4*B*). Mature AT1 cells lost their markers, including HOPX, whose expression was detected in 52% of GFP cells in the mutant lung versus 87% in the control lung ($n = 2$ mice for each genotype; >50 GFP cells/mouse), AGER, PDPN, and AQP5 (Fig. 4*C* and *SI Appendix*, Fig. S2*B*); they also regressed in size with accumulated ECAD (Fig. 4*D*), and reentered the cell cycle as measured by KI67 (Fig. 4*E*). Remarkably, 3 wk after recombination, large clusters of mutant cells were observed (*SI Appendix*, Fig. S4*D*), highlighting the proliferative potential of at least a subset of AT1 cells that perhaps arise from AT2 cells during homeostatic turnover in the mature lung (26, 28). These data suggest that NKX2-1 is necessary for the maintenance of mature AT1 cells.

NKX2-1 Represses Gastrointestinal Gene Expression in AT1 Cells. In addition to down-regulated AT1 genes, RNA-seq comparison of control and *Nkx2-1* mutant AT1 cells (Fig. 2*B*) also revealed a group of up-regulated genes that were associated with the GI tract (Fig. 5*A*, *SI Appendix*, Fig. S4*A*, and Dataset S1). Similarly, P14 whole lung RNA-seq showed sustained expression of GI genes, such as chymotrypsin (*Cym*), trefoil factor 2 (*Tff2*), cathepsin E (*Ctse*), hepatic nuclear factor 4A (*Hnf4a*), V-set and Ig domain containing 1 (*Vsig1*), and polymeric Ig receptor (*Pigr*) (Fig. 5*A*, *SI Appendix*, Fig. S4*B*, and Dataset S2). Such GI gene up-regulation was confirmed by immunostaining, which additionally revealed that mutant cells were heterogeneous, expressing all possible combinations of TFF2 and PIGR (Fig. 5*B*). These heterogeneous cells were intermixed, lacking

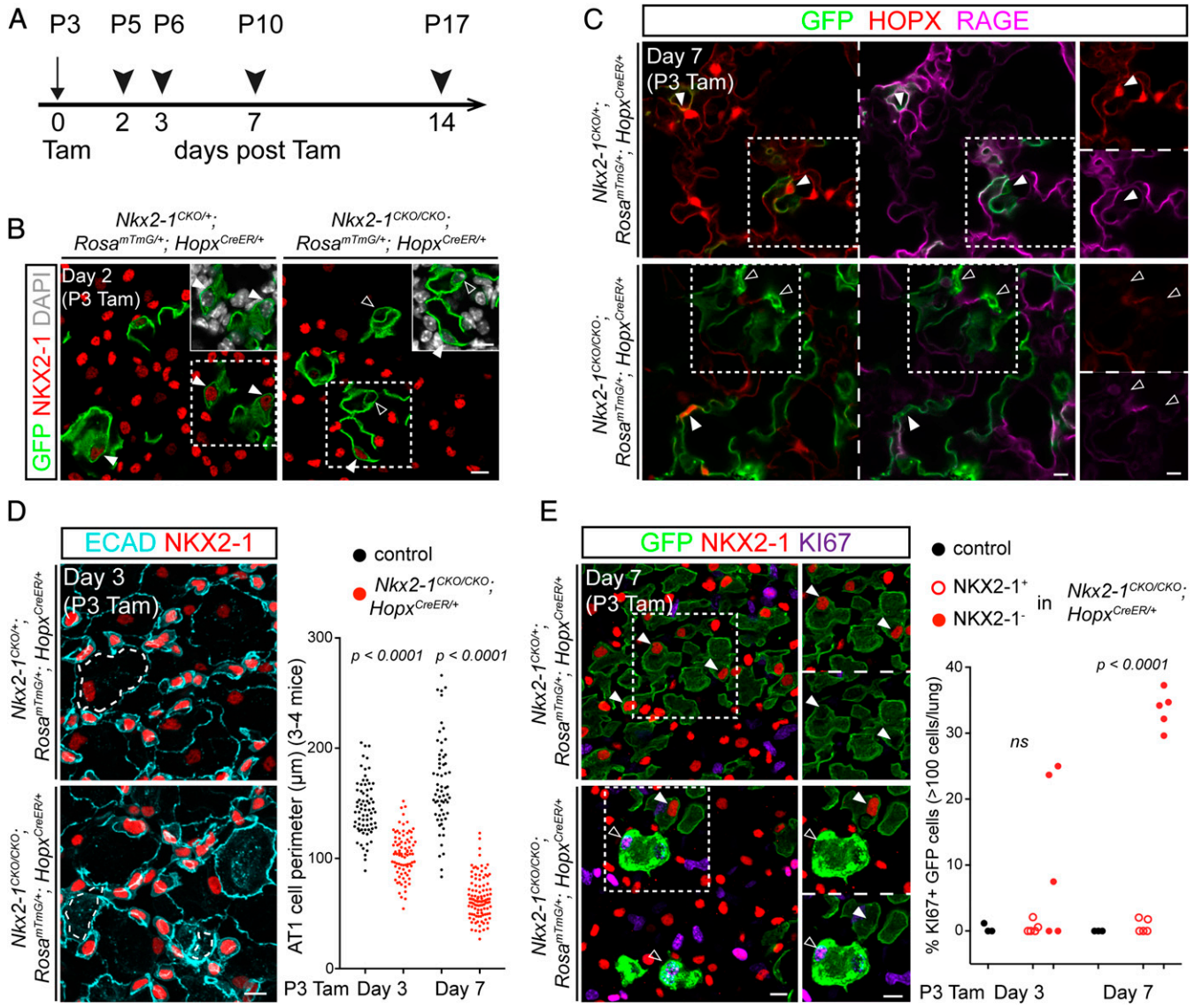

Fig. 3. *Nkx2-1* deletion leads to cell-autonomous loss of AT1 gene expression, morphology, and quiescence during development. (*A*) Timeline of tamoxifen (Tam; arrow) injection (0.25 mg) and lung harvest (arrowheads). At least 3 littermate pairs were examined at each time point with consistent results. (*B*) Optical sections of en face confocal stacks of immunostained littermate lung strips showing loss of NKX2-1 in a subset of GFP-marked AT1 cells (open versus filled arrowheads) in the mutant, but none in the control (filled arrowheads). The discrepancy in recombining the *Rosa* versus *Nkx2-1* alleles is presumably due to difference in DNA accessibility to the Cre recombinase. (*Inset*) The corresponding AT1 cell nuclei (DAPI). (*C*) Confocal images of immunostained sections from littermate lungs showing reduction of AT1 cell markers (HOPX and RAGE) in a subset of GFP-marked AT1 cells in the mutant (open versus filled arrowheads). Neighboring control AT1 cells in the mutant lung (filled arrowheads) are unaffected, but can be GFP marked as shown in *B*. (*D*) Confocal en face view of littermate lung strips showing a decrease in cell perimeter of NKX2-1 mutant AT1 cells, as outlined with ECAD (dashes) and as quantified at indicated time points with each dot representing a cell from at least 3 lungs per genotype with at least 5 images per lung (unpaired *t* test). (*E*) Confocal en face view of immunostained littermate lung strips showing KI67 expression in GFP-marked NKX2-1 mutant AT1 cells, but not GFP-marked NKX2-1 expressing control AT1 cells (open versus filled arrowheads). Each dot represents 1 lung averaged over at least 3 images (unpaired *t* test; ns, not significant). Due to discrepancy in recombining the *Rosa* and *Nkx2-1* alleles, GFP-marked NKX2-1 expressing AT1 cells in the mutant lung were quantified separately and served as internal controls. (Scale bar: 10 μm in *B*–*E*.)

the organ specificity observed in the stomach and intestines (*SI Appendix*, Fig. S4*C*). Notably, close examination using SEM and transmission electron microscopy (TEM) revealed that the *Nkx2-1* mutant lung epithelium underwent a physical transformation, forming apical structures reminiscent of the microvilli of the GI epithelium (31) (Fig. 5*C* and *SI Appendix*, Fig. S4*D*). Ectopic expression of GI genes in *Nkx2-1* mutant AT1 cells was also observed when *Nkx2-1* deletion was induced in isolated cells by $Hopx^{CreER}$ in both developing and mature AT1 cells (*SI Appendix*, Fig. S4*E*). Collectively, these data suggest that NKX2-1 is cell-autonomously required to repress GI genes.

Single-Cell RNA-Seq Reveals Transcriptome Dynamics upon Loss of *Nkx2-1*. To discern the dynamic NKX2-1–dependent transcriptional changes, we performed single-cell RNA-seq (scRNA-seq) of $Nkx2\text{-}1^{CKO/CKO}$; $Aqp5^{Cre/+}$ mutant and littermate control lungs at P10, an intermediate time point when individual AT1 cells in the mutant lung were expected to collectively feature the full range of transcriptomic phenotypes (Fig. 5*A*). We developed a cell dissociation and fluorescence-activated cell sorting protocol to purify immune, endothelial, epithelial, and mesenchymal cell lineages using CD45, ICAM2, and ECAD antibodies (*SI Appendix*, Fig. S5*A*). Using lungs with all epithelial cells genetically

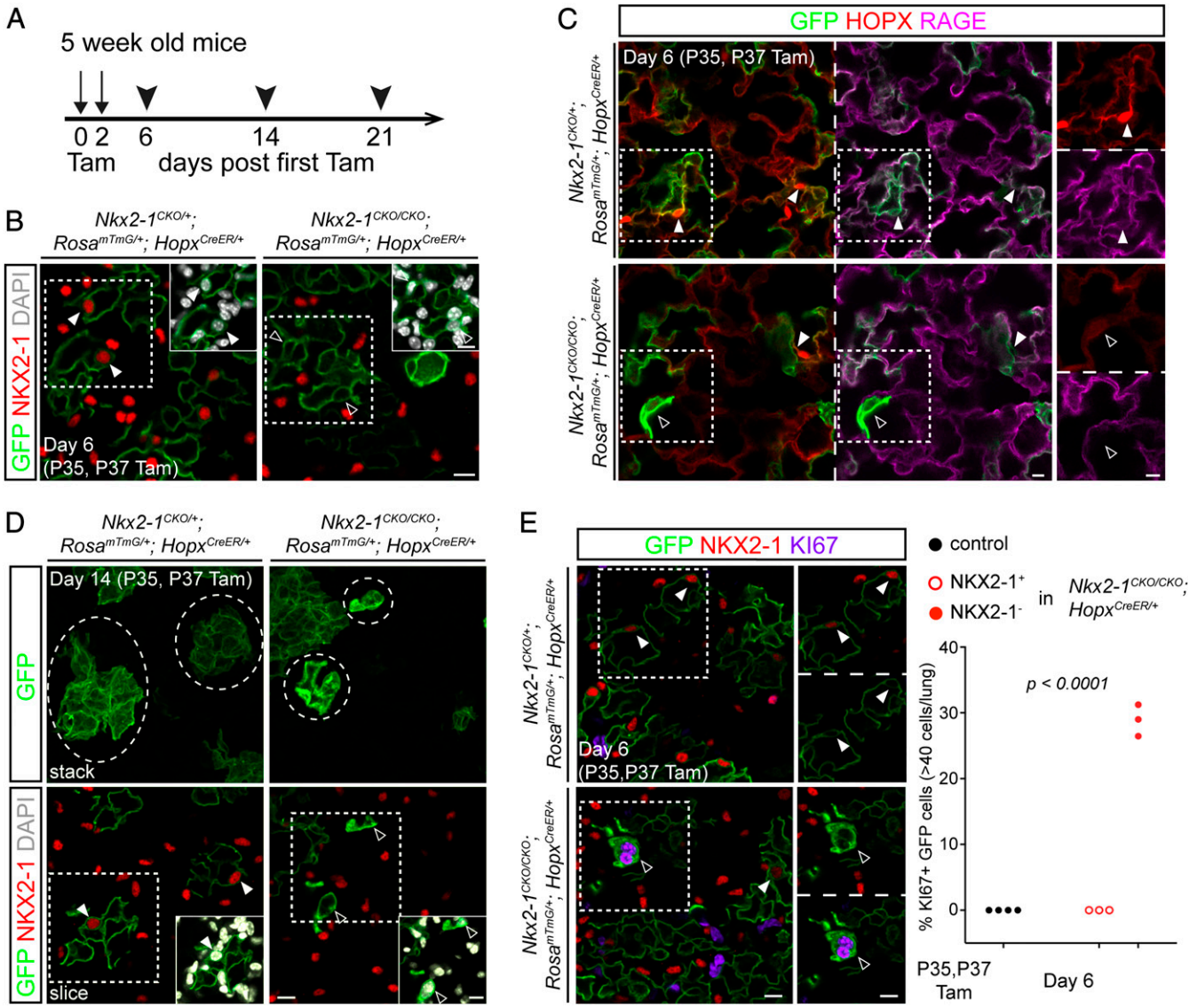

Fig. 4. NKX2-1 is required to maintain mature AT1 cell gene expression, morphology, and quiescence. (*A*) Timeline of tamoxifen (Tam; arrows) injection (3 mg) and lung harvest (arrowheads) for 5-wk-old mice. At least 3 littermate pairs were examined at each time point with consistent results. (*B*) Optical sections of en face confocal stacks of immunostained littermate lung strips showing GFP-marked NKX2-1 mutant (open arrowheads) and control (filled arrowheads) AT1 cells. (*Inset*) The corresponding AT1 cell nuclei (DAPI). (*C*) Confocal images of immunostained sections from littermate lungs showing reduction of AT1 markers (HOPX and RAGE) in a subset of GFP-marked NKX2-1 mutant AT1 cells (open versus filled arrowheads). Neighboring NKX2-1 expressing AT1 cells in the mutant lung are unaffected. (*D*, *Top*) Confocal en face view of immunostained littermate lung strips showing that GFP-marked NKX2-1 mutant AT1 cells are smaller (dash). (*D*, *Bottom*) Optical sections to show NKX2-1 in the corresponding AT1 cell nuclei (DAPI in *Insets*). Mature AT1 cells are too complex for cell perimeter quantification. (*E*) Confocal en face view of immunostained littermate lung strips showing KI67 expression in GFP-marked NKX2-1 mutant AT1 cells, but not GFP-marked NKX2-1 expressing control AT1 cells (open versus filled arrowheads). Each dot represents 1 lung averaged over at least 3 images (unpaired *t* test). Due to discrepancy in recombining the *Rosa* and *Nkx2-1* alleles, GFP-marked NKX2-1 expressing AT1 cells in the mutant lung were quantified separately and served as internal controls. (Scale bar: 10 μm in *B*–*E*.)

labeled with GFP, we verified that the ECAD and EPCAM antibodies were comparable and yielded an epithelial fraction with 92% efficiency and 84% specificity (*SI Appendix*, Fig. S5*B*). We sequenced 2,312 and 2,558 epithelial cells from control and mutant lungs, respectively, as well as nonepithelial cells that were readily identifiable by marker expression but not included in subsequent analyses (Fig. 6*A* and *SI Appendix*, Fig. S5*C*). Epithelial cells, marked by *Cdh1* (*E-cadherin*), consisted mostly of AT1 and AT2 cells in the control lung as expected (*SI Appendix*, Fig. S5*D*), whereas in the mutant lung *Nkx2-1* mutant AT1 cells, as indicated by loss of *Nkx2-1* expression, outnumbered unrecombined AT1 and AT2 cells presumably as the result of aberrant proliferation (Figs. 2*D* and 6*A*). Comparison of individual cell transcriptomes with the mouse cell atlas (32)—which contains scRNA-seq data of 400,000 cells from >40 embryonic and adult mouse tissues—confirmed the identity of control AT1 and AT2 cells, whereas mutant AT1 cells were similar to fetal intestinal epithelial cells (Fig. 6*A* and *SI Appendix*, Fig. S5*E*), supporting our bulk RNA-seq and immunostaining results (Fig. 5 and *SI Appendix*, Fig. S4). Interestingly, mutant AT1 cells were also transcriptionally similar to the principal cells of the fetal kidney collecting duct (*SI Appendix*, Fig. S5*E*), perhaps reflecting common fluid absorption function/genes (e.g., *Scnn1b*, *Scnn1g*, and *Aqp3*) among the lung, intestine, and kidney epithelial cells (33),

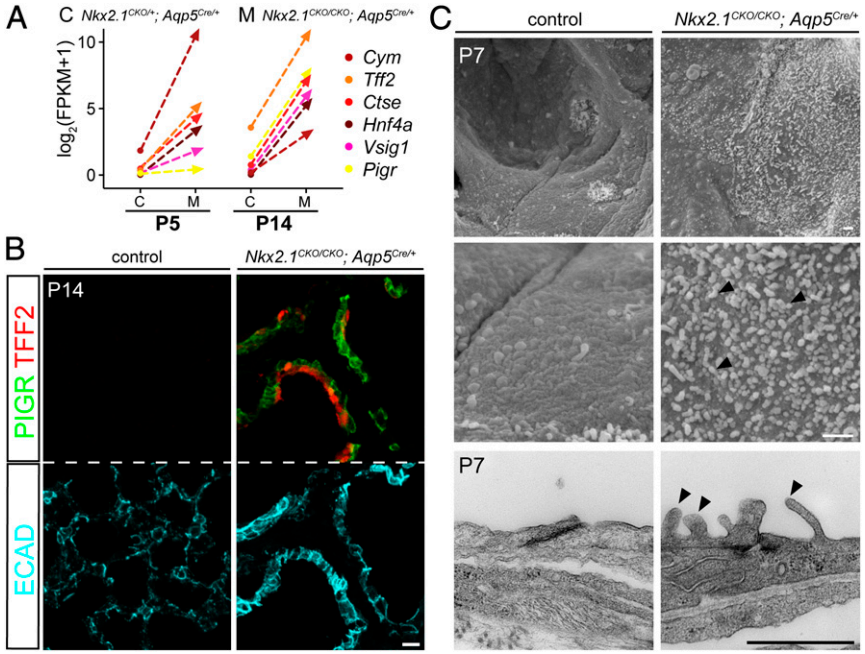

Fig. 5. NKX2-1 represses gastrointestinal gene expression in AT1 cells. (*A*) RNA-seq comparison showing up-regulation of GI genes upon *Nkx2-1* deletion in both P5 sorted GFP-marked AT1 cells averaged over 3 littermate lung pairs and P14 whole lungs from 1 littermate pair. (*B*) Confocal images of immunostained sections from littermate lungs showing ectopic GI markers (PIGR and TFF2) in the alveolar region of the *Nkx2-1* mutant lung. Three pairs of littermate lungs were examined with consistent results. (*C*) Scanning electron microscopy (*Top* 2 rows) and transmission electron microscopy (*Bottom* row) of littermate lungs showing aberrant apical microvilli-like structures (arrowheads). (Scale bar: 10 μm in *B*; 1 μm in *C*.)

although we cannot exclude the possibility of *Nkx2-1* mutant AT1 cells transforming into kidney cells despite not sharing an endodermal origin.

The nonuniform activation of GI genes (Fig. 5*B* and *SI Appendix*, Fig. S4*E*) and prior reports of diverse ectopic GI fates (34–40) prompted us to construct possible trajectories of the transcriptomic shift upon *Nkx2-1* deletion using Monocle (41–43). We found an unbranched linear trajectory connecting control AT1 cells and mutant AT1 cells expressing GI genes, suggesting that the observed heterogeneity (Fig. 5*B* and *SI Appendix*, Fig. S4*E*) was insufficient to support multiple alternative cell fates and perhaps reflected intermediate states that were either temporary or permanent during the transition from AT1 to GI fate. The trajectory analysis allowed us to stratify the top 1,000 differentially expressed genes into 5 categories based on expression dynamics and relationship to the loss of *Nkx2-1* expression (Fig. 6 *B*–*E* and Dataset S3). Specifically, early and late down-regulated genes included most of the AT1 specific genes (24 out of 27), such as *Rtkn2* and *Hopx* for the early group and *Igfbp2* and *Pdpn* for the late group. The slower decreasing kinetics of the late group could be due to perdurance, as observed for *Pdpn* (*SI Appendix*, Fig. S1*B*). Early and late up-regulated genes included GI genes, such as GST alpha 1 (*Gsta1*) for the early group and *Cym* for the late group. Activation of the early group occurred upon *Nkx2-1* loss, possibly representing initiating factors leading to the GI fate, such as *Hnf4a* expression (Fig. 6*E* and *SI Appendix*, Fig. S5*D*) (34–40). However, other key transcriptional regulators including *Pdx1* and *Cdx2* that were activated upon *Nkx2-1* deletion or *Sox2* whose ectopic expression drove esophageal differentiation in AT2 and lung tumor cells (34, 37, 38) were absent in both up-regulated groups (*SI Appendix*, Fig. S5*D* and Dataset S3), likely reflecting AT1-specific cell fate plasticity. Interestingly, some genes, which included the remaining 3 out of the 27 AT1 genes (i.e., *Akap5*, *Ahnak*, and *Lmo7*), had a biphasic pattern with a high level in the middle of the trajectory, perhaps reflecting the net activity of AT1 versus GI-specific regulatory elements of the same gene. Other biphasic genes included neutrophil genes, such as *Ly6g* and *S100a8*, likely due to a technical artifact of cell doublets that were arbitrarily assigned to the middle of the trajectory by Monocle. Taken together, NKX2-1 promotes AT1 cell fate; its loss in AT1 cells leads to a linear transition to a fate similar to fetal intestines.

NKX2-1 Binds Near AT1 Cell Genes in the Lung. To determine how DNA binding contributed to NKX2-1–dependent transcriptional changes, we performed ChIP-seq in P10 lungs using 4 independent NKX2-1 antibodies. Binding was consistent across antibodies throughout the genome including previously characterized *Nkx2-1* and *Sftpb* promoters (*SI Appendix*, Fig. S6 *A*–*C*). Motif analysis of the resulting DNA binding sites identified the known NKX2-1 consensus binding motif as the top hit (*SI Appendix*, Fig. S6*E*). Further analysis was done using data from 2 antibodies: an Abcam antibody (cat. no. 133737) due to its higher protein concentration and better performance based on ENCODE standards (44) (*SI Appendix*, Fig. S7*C*) and a Millipore antibody (cat. no. 07-601) that was previously used in ChIP experiments (45). NKX2-1 binding peaks with the highest score represented 62% of all reproducible peaks, supporting high data quality, and were mapped using the nearest-gene method to 28% of all genes in the mm10 genome, supporting a global transcriptional function of NKX2-1 (Fig. 7*B*, *SI Appendix*, Fig. S6*D*, and Dataset S4). When correlated to the 5 expression categories in the trajectory analysis (Fig. 6*E*), NKX2-1 binding sites were mapped to 65%, 75%, and 50% of early and late down-regulated and biphasic genes, respectively, a significant enrichment over the average genome (Fig. 7 *A* and *B*). Notably, 93% of the 27 AT1 genes had NKX2-1 binding sites, supporting a direct and near-universal role of NKX2-1 in promoting AT1 genes. In contrast to this high proportion of NKX2-1 binding to AT1 genes, only 41% of early up-regulated genes and 28% of late up-regulated genes had NKX2-1 binding sites—a small difference from the average genome that disappeared when taking into account the number

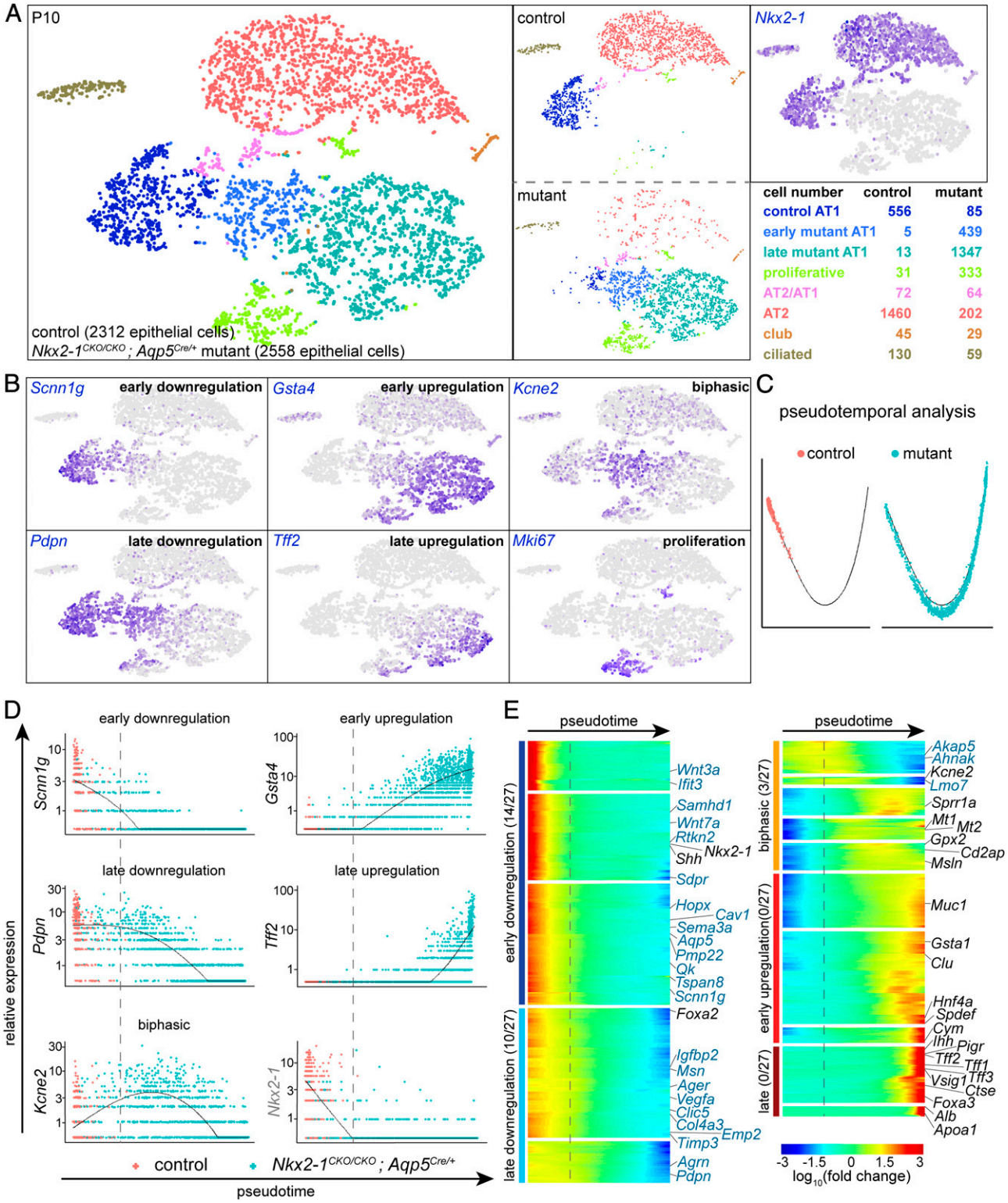

Fig. 6. Single-cell RNA-seq analysis identifies 5 patterns of differential gene expression upon *Nkx2-1* deletion. (*A*) Seurat t-distributed stochastic neighbor embedding (tSNE) plots of sorted epithelial cells from littermate lungs (merged and split views in the 2 *Left* columns). Most epithelial cells in the mutant lung do not express *Nkx2-1* (*Top* in the *Rightmost* column). Color-coded cell types are tabulated and identified using the following markers: control AT1, *Aqp5*; mutant AT1, *Nkx2-1* negative (early mutant AT1 is closer to control AT1 spatially in the tSNE plot); proliferative, *Mki67* (*B*); AT2/AT1, coexpression of *Lamp3* and *Aqp5*; AT2, *Lamp3*; club, *Scgb1a1*; and ciliated, *Foxj1*. See *SI Appendix*, Fig. S5*D*. (*B*) Representative genes for each pattern of differential gene expression. Early up-/down-regulated genes exhibit changes in the early mutant AT1 cluster, whereas late up-/down-regulated genes exhibit changes in the late mutant AT1 cluster. The biphasic genes are first up-regulated and then down-regulated as control AT1 cells transition to early and then late mutant AT1 cells. (*C*) Monocle pseudotemporal analysis of AT1 cells from control and mutant lungs, excluding *Mki67* cells. (*D*) Pseudotemporal changes of representative genes for the 5 patterns of differential gene expression. Vertical dashes demarcate loss of *Nkx2-1* expression (also in *E*). (*E*) Heatmap of pseudotime-dependent gene clusters from the top 1,000 differentially expressed genes. *Nkx2-1* loss is marked by vertical dashes. A total of 24 out of 27 AT1 cell-specific genes (blue gene names) are in the down-regulated groups.

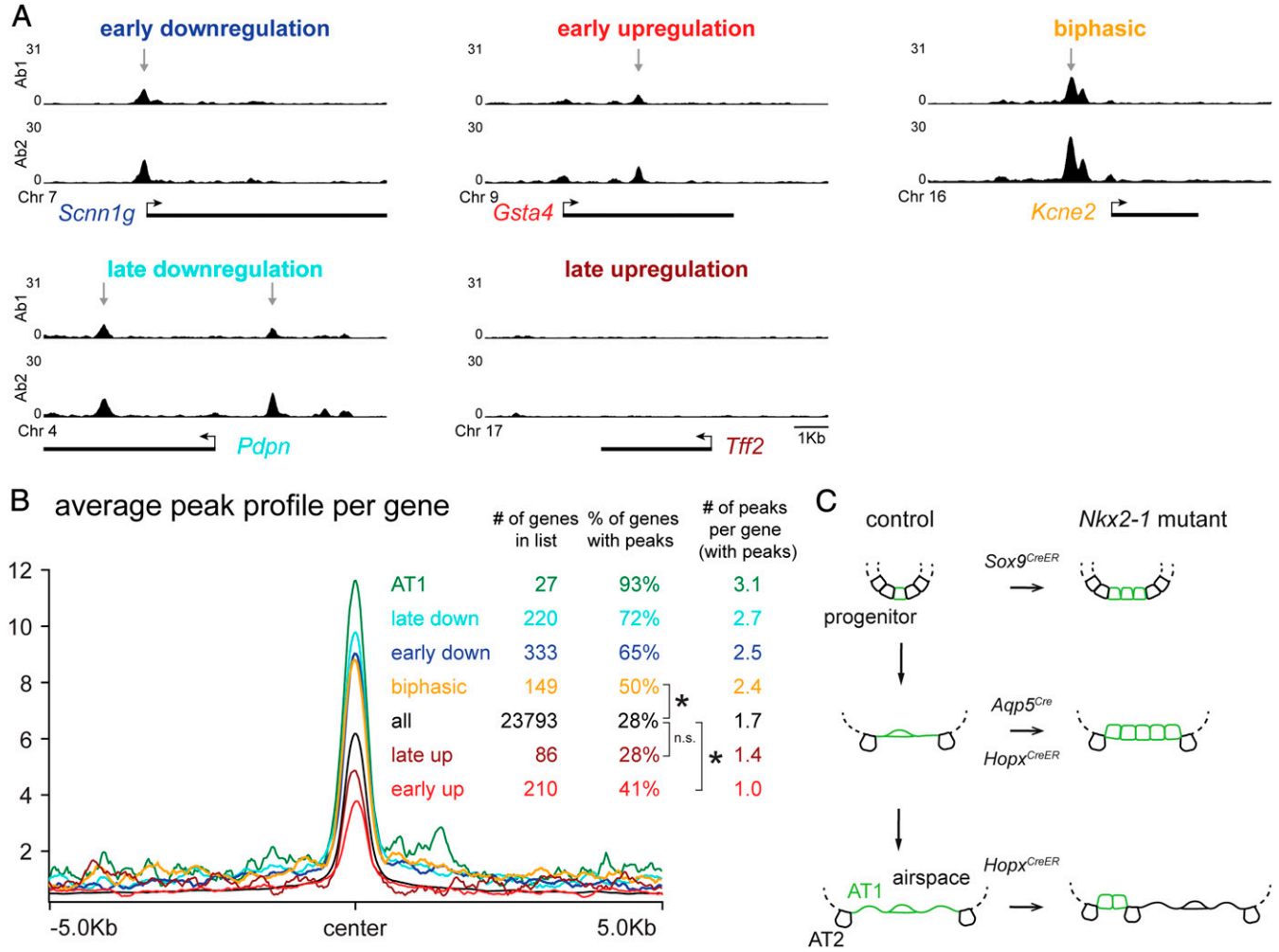

Fig. 7. NKX2-1 binds near AT1 and down-regulated genes. (*A*) NKX2-1 ChIP peaks (gray arrows) near genes representative of the 5 patterns of differential gene expression (Fig. 6) using wild-type P10 lungs and 2 independent antibodies (Ab1, Abcam ab133737; Ab2, Millipore 07-601). (*B*) Average (per gene) NKX2-1 ChIP peak profiles that are color coded as in *A* and tabulated in the order of peak height. The 27-AT1 gene group has the highest average binding. The whole genome (all; 23,793 genes) serves as a reference for background binding. Asterisks: $P < 0.0001$; n.s., not significant (χ^2 test). (*C*) A model summarizing the 4 deletion models and showing that *Nkx2-1* is required for the specification, development, and maintenance of AT1 cells (green).

of peaks for each gene and the number of sequencing reads for each peak (Fig. 7 *A* and *B*), suggesting that NKX2-1 indirectly represses GI genes.

NKX2-1 Is Necessary for AT2 Cell Development. As a comparison, we also examined the role of NKX2-1 during AT2 cell development by deleting it at P4 with *Sftpc*^{CreER} (46), which, even at a very low dose of tamoxifen (0.5 μg), targeted AT2 cells with an efficiency of 63% and a specificity of 98% within the alveolar epithelium, based on the *Rosa*^{Sun1GFP} reporter ($n = 3$ mice; >300 cells/mouse). We used this limited dose of tamoxifen because a higher amount led to animal death within 5 d, presumably due to insufficient surfactant production at a critical stage of lung maturation as described below. In this limited deletion model (*SI Appendix*, Fig. S7*A*), NKX2-1 was lost in 5% of GFP-expressing AT2 cells ($n = 3$ mice; >500 GFP cells/mouse) (*SI Appendix*, Fig. S7*B*). Within 8 d of recombination, mutant cells down-regulated AT2 markers including surfactant protein C (SFTPC) and LAMP3 (*SI Appendix*, Fig. S7*C*) and also proliferated and formed clusters, whereas control AT2 cells had a much lower level of proliferation at P12 and became nearly quiescent at P18 as the lung matured (*SI Appendix*, Fig. S7 *C* and *D*). Furthermore, mutant AT2 cells ectopically expressed GI genes (*SI Appendix*, Fig. S7*E*). To fully characterize the mutant AT2 cells and overcome the confounding issue of mosaic deletion, we induced recombination with a high dose of tamoxifen (300 μg) and sorted GFP cells for RNA-seq 3 d later before animal death. We found that mutant cells down-regulated 23 out of 24 AT2 genes that we compiled from the literature (27, 47), such as *Sftpc*, *Lamp3*, *Slc34a2*, and *Abca3*, and up-regulated GI genes, such as *Tff2*, *Cym*, *Ctse*, and *Hnf4a*, confirming our immunostaining results (*SI Appendix*, Fig. S7*F* and Dataset S5). These data indicate that NKX2-1 is also required for AT2 cell development but it regulates a set of AT2 cell-specific genes that are distinct from those of AT1 cells (*SI Appendix*, Fig. S7*G*).

Discussion

In this study, we demonstrate that NKX2-1 is expressed by AT1 cells and is essential at all stages of AT1 cells including their specification, development, and maintenance (Fig. 7*C*). This pivotal role of NKX2-1 results from its regulation of 3 defining features of AT1 cells: cell type-specific gene expression, morphology, and quiescence. Furthermore, without NKX2-1, AT1 cells adopt a GI fate, illustrating remarkable plasticity of an otherwise terminally differentiated and highly specialized cell type. Our single-cell and genomic analysis of NKX2-1 target genes

provides a foundation to unravel the transcriptional control of the poorly understood AT1 cell.

The 3 NKX2-1–dependent features—AT1 cell-specific genes, morphology, and quiescence—are likely to be intertwined. On one hand, NKX2-1 binds to a group of AT1 cell-specific genes, such as *Rtkn2*, *Pmp22*, *Akap5*, and *Emp2*, that have been implicated in regulating the cytoskeleton, membrane composition, and extracellular matrix (48–52) and thus could impact the ultrathin, expansive morphology of AT1 cells. On the other hand, the complete regression to a columnar shape might be a prerequisite to or a result of cell division. However, cell cycle reentry, as based on KI67 expression, and the binuclear profile are apparent at the beginning of cell shrinkage and before complete loss of AT1 cell-specific genes (Fig. 2), suggesting a direct role of NKX2-1 in maintaining cellular quiescence. If true, NKX2-1 undergoes a shift from proproliferation during early branching morphogenesis (20, 21, 45), to antiproliferation upon AT1 cell differentiation, highlighting the importance of cellular states.

The transformation of *Nkx2-1* mutant AT1 cells to the GI fate is drastic—forming microvilli-like apical protrusions (Fig. 5*C* and *SI Appendix*, Fig. S4*D*) and starting from fully differentiated AT1 cells (*SI Appendix*, Fig. S4*E*). Such transformation is nevertheless incomplete with a transcriptome resembling the fetal, but not mature, intestinal cells (*SI Appendix*, Fig. S5*E*) and with cells possibly stalled along a linear trajectory of cell fate conversion (Fig. 6*C*), perhaps reflecting a passive drift to an alternative endodermal fate in the absence of NKX2-1. Consistent with this idea, NKX2-1 binding to the derepressed GI genes is not above the whole genome average, in sharp contrast with the 93% binding rate for AT1 genes (Fig. 7*B*). Similar GI transformation is also reported for *Nkx2-1* mutant AT2 cells and lung tumor cells, possibly as the result of ectopic transcriptional activation by FOXA1/2 that are freed from their normal partner NKX2-1 (35, 37). However, *Nkx2-1* mutant AT1 cells are notably different from mutant AT2 cells in that the former do not express *Pdx1* nor do they have uniform *Hnf4a* expression, suggesting that cell of origin influences the repertoire of activatable GI genes.

Our study paints a fuller picture of NKX2-1 function in the lung, including its progenitors and AT1 and AT2 cells, as well as other organs, including the thyroid and the brain (24, 53–60). In each case, NKX2-1 promotes a distinct set of cell type-specific genes, emphasizing the importance of cellular contexts that may include unique transcriptional cofactors, chromatin states affecting NKX2-1 binding or lineage potentials, protein isoforms or modifications such as phosphorylation (61–63). A thorough comparison of the roles of NKX2-1 in AT1 versus AT2 cells using precise genetic models and emerging single-cell genomic and epigenomic tools promises an experimental paradigm to study how a common lineage transcription factor exerts cell type-specific functions.

Methods

Mouse strains and antibodies were acquired from academic laboratories and commercial sources as detailed in *SI Appendix*. Animal experiments were approved by the Institutional Animal Care and Use at Texas A&M Health Science Center Institute of Biosciences and Technology and MD Anderson Cancer Center. Immunostaining, electron microscopy, cell sorting, and bulk RNA-seq were performed as published with minor modifications (5). See *SI Appendix* for details on image analysis and cell quantification. ChIP-seq and scRNA-seq including data analysis are described in *SI Appendix*. Raw genomic data were deposited in GEO under the accession no. GSE129628 (64).

ACKNOWLEDGMENTS. We thank Kenneth Dunner Jr. for help with SEM and TEM. We would also like to thank Dr. Richard Behringer for his suggestions. This work was supported by the University of Texas MD Anderson Cancer Center institutional research grant and start-up funds, NIH R01HL130129 (J.C.), F31HL139095 (D.R.L.), and R35HL135747 (Z.B.), and Cancer Center Support Grant CA 16672.

1. E. E. Morrisey, B. L. Hogan, Preparing for the first breath: Genetic and cellular mechanisms in lung development. *Dev. Cell* **18**, 8–23 (2010).
2. E. R. Weibel, On the tricks alveolar epithelial cells play to make a good lung. *Am. J. Respir. Crit. Care Med.* **191**, 504–513 (2015).
3. E. R. Weibel, The mystery of "non-nucleated plates" in the alveolar epithelium of the lung explained. *Acta Anat. (Basel)* **78**, 425–443 (1971).
4. J. Yang, J. Chen, Developmental programs of lung epithelial progenitors: A balanced progenitor model. *Wiley Interdiscip. Rev. Dev. Biol.* **3**, 331–347 (2014).
5. J. Yang *et al.*, The development and plasticity of alveolar type 1 cells. *Development* **143**, 54–65 (2016).
6. J. Li *et al.*, The strength of mechanical forces determines the differentiation of alveolar epithelial cells. *Dev Cell* **44**, 297–312.e5 (2018).
7. M. Loscertales *et al.*, Type IV collagen drives alveolar epithelial-endothelial association and the morphogenetic movements of septation. *BMC Biol.* **14**, 59 (2016).
8. X. Wang *et al.*, Expression of histone deacetylase 3 instructs alveolar type I cell differentiation by regulating a Wnt signaling niche in the lung. *Dev. Biol.* **414**, 161–169 (2016).
9. T. J. Desai, D. G. Brownfield, M. A. Krasnow, Alveolar progenitor and stem cells in lung development, renewal and cancer. *Nature* **507**, 190–194 (2014).
10. D. B. Frank *et al.*, Emergence of a wave of Wnt signaling that regulates lung alveologenesis by controlling epithelial self-renewal and differentiation. *Cell Rep.* **17**, 2312–2325 (2016).
11. Y. Wang *et al.*, HDAC3-dependent epigenetic pathway controls lung alveolar epithelial cell remodeling and spreading via miR-17-92 and TGF-β signaling regulation. *Dev. Cell* **36**, 303–315 (2016).
12. L. B. Nantie *et al.*, *Lats1/2* inactivation reveals Hippo function in alveolar type I cell differentiation during lung transition to air breathing. *Development* **145**, dev163105 (2018).
13. C. Lin, E. Yao, P. T. Chuang, A conserved MST1/2-YAP axis mediates Hippo signaling during lung growth. *Dev. Biol.* **403**, 101–113 (2015).
14. A. W. Lange *et al.*, Hippo/Yap signaling controls epithelial progenitor cell proliferation and differentiation in the embryonic and adult lung. *J. Mol. Cell Biol.* **7**, 35–47 (2015).
15. Z. Borok, A. Hami, S. I. Danto, S. M. Zabski, E. D. Crandall, Rat serum inhibits progression of alveolar epithelial cells toward the type I cell phenotype in vitro. *Am. J. Respir. Cell Mol. Biol.* **12**, 50–55 (1995).
16. K. Ikeda *et al.*, Gene structure and expression of human thyroid transcription factor-1 in respiratory epithelial cells. *J. Biol. Chem.* **270**, 8108–8114 (1995).
17. J. M. Liebler *et al.*, Combinations of differentiation markers distinguish subpopulations of alveolar epithelial cells in adult lung. *Am. J. Physiol. Lung Cell. Mol. Physiol.* **310**, L114–L120 (2016).
18. B. D. Harfe *et al.*, Evidence for an expansion-based temporal Shh gradient in specifying vertebrate digit identities. *Cell* **118**, 517–528 (2004).
19. A. Mo *et al.*, Epigenomic signatures of neuronal diversity in the mammalian brain. *Neuron* **86**, 1369–1384 (2015).
20. P. Minoo *et al.*, TTF-1 regulates lung epithelial morphogenesis. *Dev. Biol.* **172**, 694–698 (1995).
21. P. Minoo, C. Li, H. B. Liu, H. Hamdan, R. deLemos, TTF-1 is an epithelial morphoregulatory transcriptional factor. *Chest* **111** (suppl. 6), 135S–137S (1997).
22. P. Minoo, G. Su, H. Drum, P. Bringas, S. Kimura, Defects in tracheoesophageal and lung morphogenesis in Nkx2.1(-/-) mouse embryos. *Dev. Biol.* **209**, 60–71 (1999).
23. P. Flodby *et al.*, Directed expression of Cre in alveolar epithelial type 1 cells. *Am. J. Respir. Cell Mol. Biol.* **43**, 173–178 (2010).
24. T. Kusakabe *et al.*, Thyroid-specific enhancer-binding protein/NKX2.1 is required for the maintenance of ordered architecture and function of the differentiated thyroid. *Mol. Endocrinol.* **20**, 1796–1809 (2006).
25. M. Heiman *et al.*, A translational profiling approach for the molecular characterization of CNS cell types. *Cell* **135**, 738–748 (2008).
26. Y. Wang *et al.*, Pulmonary alveolar type I cell population consists of two distinct subtypes that differ in cell fate. *Proc. Natl. Acad. Sci. U.S.A.* **115**, 2407–2412 (2018).
27. B. Treutlein *et al.*, Reconstructing lineage hierarchies of the distal lung epithelium using single-cell RNA-seq. *Nature* **509**, 371–375 (2014).
28. R. Jain *et al.*, Plasticity of Hopx(+) type I alveolar cells to regenerate type II cells in the lung. *Nat. Commun.* **6**, 6727 (2015).
29. M. D. Muzumdar, B. Tasic, K. Miyamichi, L. Li, L. Luo, A global double-fluorescent Cre reporter mouse. *Genesis* **45**, 593–605 (2007).
30. T. Soeda *et al.*, Sox9-expressing precursors are the cellular origin of the cruciate ligament of the knee joint and the limb tendons. *Genesis* **48**, 635–644 (2010).
31. K. I. Pinson, L. Dunbar, L. Samuelson, D. L. Gumucio, Targeted disruption of the mouse villin gene does not impair the morphogenesis of microvilli. *Dev. Dyn.* **211**, 109–121 (1998).
32. X. Han *et al.*, Mapping the mouse cell atlas by microwell-seq. *Cell* **173**, 1307 (2018).
33. L. Chen *et al.*, Transcriptomes of major renal collecting duct cell types in mouse identified by single-cell RNA-seq. *Proc. Natl. Acad. Sci. U.S.A.* **114**, E9989–E9998 (2017).
34. P. R. Tata *et al.*, Developmental history provides a roadmap for the emergence of tumor plasticity. *Dev Cell* **44**, 679–693.e5 (2018).
35. S. A. Camolotto *et al.*, FoxA1 and FoxA2 drive gastric differentiation and suppress squamous identity in NKX2-1-negative lung cancer. *eLife* **7**, e38579 (2018).
36. G. Mollaoglu *et al.*, The lineage-defining transcription factors SOX2 and NKX2-1 determine lung cancer cell fate and shape the tumor immune microenvironment. *Immunity* **49**, 764–779e9 (2018).

37. E. L. Snyder *et al*., Nkx2-1 represses a latent gastric differentiation program in lung adenocarcinoma. *Mol. Cell* **50**, 185–199 (2013).
38. C. M. Li *et al*., Foxa2 and Cdx2 cooperate with Nkx2-1 to inhibit lung adenocarcinoma metastasis. *Genes Dev.* **29**, 1850–1862 (2015).
39. M. J. Herriges *et al*., The NANCI-Nkx2.1 gene duplex buffers Nkx2.1 expression to maintain lung development and homeostasis. *Genes Dev.* **31**, 889–903 (2017).
40. Y. Maeda *et al*., Kras(G12D) and Nkx2-1 haploinsufficiency induce mucinous adenocarcinoma of the lung. *J. Clin. Invest.* **122**, 4388–4400 (2012).
41. C. Trapnell *et al*., The dynamics and regulators of cell fate decisions are revealed by pseudotemporal ordering of single cells. *Nat. Biotechnol.* **32**, 381–386 (2014).
42. X. Qiu *et al*., Single-cell mRNA quantification and differential analysis with Census. *Nat. Methods* **14**, 309–315 (2017).
43. X. Qiu *et al*., Reversed graph embedding resolves complex single-cell trajectories. *Nat. Methods* **14**, 979–982 (2017).
44. S. G. Landt *et al*., ChIP-seq guidelines and practices of the ENCODE and modENCODE consortia. *Genome Res.* **22**, 1813–1831 (2012).
45. J. B. Tagne *et al*., Genome-wide analyses of Nkx2-1 binding to transcriptional target genes uncover novel regulatory patterns conserved in lung development and tumors. *PLoS One* **7**, e29907 (2012).
46. J. R. Rock *et al*., Multiple stromal populations contribute to pulmonary fibrosis without evidence for epithelial to mesenchymal transition. *Proc. Natl. Acad. Sci. U.S.A.* **108**, E1475–E1483 (2011).
47. M. F. Beers, Y. Moodley, When is an alveolar type 2 cell an alveolar type 2 cell? A conundrum for lung stem cell biology and regenerative medicine. *Am. J. Respir. Cell Mol. Biol.* **57**, 18–27 (2017).
48. E. J. Lee *et al*., Epithelial membrane protein 2 regulates sphingosylphosphorylcholine-induced keratin 8 phosphorylation and reorganization: Changes of PP2A expression by interaction with alpha4 and caveolin-1 in lung cancer cells. *Biochim. Biophys. Acta* **1863**, 1157–1169 (2016).
49. L. A. Bruggeman, S. Martinka, J. S. Simske, Expression of TM4SF10, a Claudin/EMP/PMP22 family cell junction protein, during mouse kidney development and podocyte differentiation. *Dev. Dyn.* **236**, 596–605 (2007).
50. C. Lopez-Anido *et al*., Tead1 regulates the expression of peripheral myelin protein 22 during Schwann cell development. *Hum. Mol. Genet.* **25**, 3055–3069 (2016).
51. G. Rosso, P. Young, V. Shahin, Implications of schwann cells biomechanics and mechanosensitivity for peripheral nervous system physiology and pathophysiology. *Front. Mol. Neurosci.* **10**, 345 (2017).
52. M. Weisenhaus *et al*., Mutations in AKAP5 disrupt dendritic signaling complexes and lead to electrophysiological and behavioral phenotypes in mice. *PLoS One* **5**, e10325 (2010).
53. L. Magno *et al*., NKX2-1 is required in the embryonic septum for cholinergic system development, learning, and memory. *Cell Rep.* **20**, 1572–1584 (2017).
54. L. Magno *et al*., The integrity of cholinergic basal forebrain neurons depends on expression of Nkx2-1. *Eur. J. Neurosci.* **34**, 1767–1782 (2011).
55. T. Kusakabe, N. Hoshi, S. Kimura, Origin of the ultimobranchial body cyst: T/ebp/Nkx2.1 expression is required for development and fusion of the ultimobranchial body to the thyroid. *Dev. Dyn.* **235**, 1300–1309 (2006).
56. S. Liang *et al*., A branching morphogenesis program governs embryonic growth of the thyroid gland. *Development* **145**, dev146829 (2018).
57. S. Minocha *et al*., Nkx2.1 regulates the generation of telencephalic astrocytes during embryonic development. *Sci. Rep.* **7**, 43093 (2017).
58. M. Sandberg *et al*., Transcriptional networks controlled by NKX2-1 in the development of forebrain GABAergic neurons. *Neuron* **91**, 1260–1275 (2016).
59. C. L. Yee, Y. Wang, S. Anderson, M. Ekker, J. L. Rubenstein, Arcuate nucleus expression of NKX2.1 and DLX and lineages expressing these transcription factors in neuropeptide Y(+), proopiomelanocortin(+), and tyrosine hydroxylase(+) neurons in neonatal and adult mice. *J. Comp. Neurol.* **517**, 37–50 (2009).
60. E. J. Ostrin *et al*., β-Catenin maintains lung epithelial progenitors after lung specification. *Development* **145**, dev160788 (2018).
61. C. Li, J. Cai, Q. Pan, P. Minoo, Two functionally distinct forms of NKX2.1 protein are expressed in the pulmonary epithelium. *Biochem. Biophys. Res. Commun.* **270**, 462–468 (2000).
62. V. Kolla *et al*., Thyroid transcription factor in differentiating type II cells: Regulation, isoforms, and target genes. *Am. J. Respir. Cell Mol. Biol.* **36**, 213–225 (2007).
63. D. Silberschmidt *et al*., In vivo role of different domains and of phosphorylation in the transcription factor Nkx2-1. *BMC Dev. Biol.* **11**, 9 (2011).
64. D. R. Little *et al*., Transcriptional control of lung alveolar type 1 cell development and maintenance by NK homeobox 2-1. Gene Expression Omnibus. https://www.ncbi.nlm.nih.gov/geo/query/acc.cgi?acc=GSE129628. Deposited 8 August 2019.